Microporous and Mesoporous Materials 394 (2025) 113663

Contents lists available at ScienceDirect

Microporous and Mesoporous Materials

journal homepage: www.elsevier.com/locate/micromeso

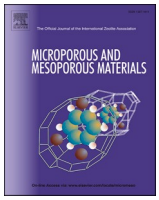

Targeted micronutrient nanofertilizers of injectable actions based on Cu/B/I halloysite nanotube composites

Evan Dasi [a], Ivan Khitrin [a], Alexey Ruban [a], Prokopiy Maximov [a], Natalia Maximova [a], Peng Yuan [b], Maxim Rudmin [a,*]

[a] Division for Geology, School of Earth Sciences & Engineering, Tomsk Polytechnic University, Tomsk, 634050, Russia
[b] School of Environmental Science and Engineering, Guangdong University of Technology, Guangzhou, 510006, China

ARTICLE INFO

Keywords:
Halloysite
Nanotubes
Nanocomposites
Micronutrients
Targeted fertilizers

ABSTRACT

The development of modern fertilizers includes the creation of various eco-friendly composites made from mineral or organic substance carrier combined with nutrient fillers. This study aims to design targeted micronutrient nanofertilizers with injectable properties by chemically activating halloysite nanotubes as carrier. The goal is to analyze the sorption of copper (Cu), boron (B), and iodine (I) on the meso- and micropores of halloysite to enhance their performance. Halloysite nanotubes were modified via intercalation and adsorption of aqueous solutions containing chelated copper, boric acid, or iodine solutions. As a result, nanotube composites with different concentrations were produced. The encapsulation of Cu/B/I in halloysite, as well as the modification of the nanotubes, was investigated using various techniques, including SEM with EDS, BET surface area analysis, TEM with SAED, TG-DSC with MS, and ICP-MS. Laboratory plant growth tests were conducted, along with detailed observations of how the composites affected the leaf surface, to analyze the effectiveness of the designed fertilizers. Copper, boron, and iodine were intercalated in the micropore space of the halloysite. As the concentration of the reacted solution increased, the average outer diameter of the nanotubes increased up to 300 nm, indicating that the macropore space, also known as the "site," was filled. The results of the plant growth tests revealed a strong adhesion of activated halloysite nanotubes to arugula microgreens and a stimulating effect of the created composites on height and yield, which increased by up to 34 %. This phenomenon guarantees that the fertilizer remains on the plant's surface for an extended period and is less likely to wash away due to irrigation or rain. Surface spraying of halloysite nanotubes allows for the accurate delivery of micronutrients to plants while preventing soil and groundwater contamination, making this fertilizer ecologically sound. The proposed method of activating halloysite with Cu, B, and I solutions is promising and could lead to the development of fertilizers in the near future.

1. Introduction

Micronutrient fertilizers are important for increasing crop yields and improving soil quality by providing essential nutrients that plants can easily absorb [1–3]. However, traditional fertilizers often face problems like quick leaching, low nutrient use efficiency, and environmental losses. Targeted nanofertilizers have emerged as a promising solution. These nanofertilizers offer controlled nutrient release and improved bioavailability [4–9].

Halloysite nanotubes have attracted significant attention among the various nanocarriers for these composites. This interest is due to their unique layered tubular structure, high surface area, and ability to encapsulate and gradually release a range of substances [10–13].

Halloysite is a phyllosilicate clay mineral known for its layered crystal structure and remarkable flexibility [14]. This naturally occurring aluminosilicate clay mineral features a unique hollow tubular morphology, setting it apart from conventional layered silicates [11,15–19]. These characteristics make halloysite versatile and applicable in various scientific and industrial fields [10,20].

One of the most defining features of halloysite nanotubes is their high aspect ratio, which describes the relationship between their length and diameter [21]. These nanotubes typically have an aspect ratio of

* Corresponding author.
E-mail addresses: de01@tpu.ru (E. Dasi), ish9@tpu.ru (I. Khitrin), ruban@tpu.ru (A. Ruban), pnm1@tpu.ru (P. Maximov), nak58@tpu.ru (N. Maximova), yuanpeng@gdut.edu.cn (P. Yuan), rudminma@tpu.ru (M. Rudmin).

https://doi.org/10.1016/j.micromeso.2025.113663
Received 2 March 2025; Received in revised form 21 April 2025; Accepted 25 April 2025
Available online 29 April 2025

10:1 or higher, resulting in an elongated, needle-like shape [10,21–28]. This hollow structure enhances their exceptional loading and encapsulation capabilities, making them ideal candidates for drug delivery systems [27,29–37].

Halloysite nanotubes have remarkable chemical and thermal stability, which makes them suitable for a variety of applications [21,38,39]. They can endure both acidic and alkaline conditions. Their resistance to high temperatures makes them ideal for various industrial applications, including catalysis and the manufacturing of polymer nanocomposites [40–42]. Furthermore, the exterior surface of halloysite nanotubes can be easily modified to introduce specific functionalities or coatings [21,43–47].

This study aims to develop and characterize copper/boron/iodine (Cu/B/I)-modified halloysite nanotube nanocomposites to serve as a targeted micronutrient fertilizer with injectable properties. The modification enhanced nutrient loading capacity, optimized release kinetics, and improved plant bioavailability. The agronomic performance of the developed nanocomposites was evaluated through laboratory-scale bioassays using arugula microgreens (*Eruca sativa*). This work provides new insights into the development of next-generation targeted nanofertilizers, highlighting the potential of halloysite-based carriers for sustainable and resource-efficient agriculture.

2. Materials and methods

2.1. Materials

Halloysite nanotubes (HNTs) concentrate supplied by Halloysite-Ural LLC (Chelyabinsk, Russia) was used as a mineral material. Chelated copper, boron acid, and iodine were chosen as the active components to obtain nanocomposites. These compounds were selected due to their essential role in plant nutrition and their ability to interact with the tubular structure of halloysite.

Aqueous solutions of chelated copper (5, 20, and 40 wt%), boric acid (5, 20, and 40 wt%), and potassium iodide (5, 20, and 40 wt%) were prepared and used for nanocomposite synthesis.

2.2. Chemical preparation of nanocomposites

Nanocomposites were synthesized by impregnating halloysite nanotubes with chelated copper, boric acid, and potassium iodide. The purpose of this process was to introduce micronutrients into the nanostructure of halloysite through adsorption and intercalation.

Each halloysite sample (60–95 g) was mixed with a specific volume of nutrient solution (40 ml) and left for 48 h at room temperature to ensure complete absorption. The 48-h incubation period was selected based on preliminary experiments and literature precedents [48,49] indicating that similar durations are sufficient for achieving adsorption equilibrium under static conditions. After impregnation, the suspensions were not washed to preserve weakly bound nutrient species that may contribute to bioavailability. The excess unabsorbed solution was removed during subsequent drying. The resulting nanocomposites were then dried in a vacuum oven at 60 °C for 24 h before characterization (Table 1).

Table 1
Characterization of preparation of halloysite-based nanocomposites.

Nanocomposite	Preparation formula
Hly3Cu2-40	60 g of HNTs +40 ml of a solution with a copper-chelated concentration of 40 %
Hly3Cu2-20	60 g of HNTs +40 ml of a solution with a copper-chelated concentration of 20 %
Hly3Cu2-05	60 g of HNTs +40 ml of a solution with a copper-chelated concentration of 5 %
Hly3B2-40	60 g of HNTs +40 ml of a solution with a boron concentration of 40 %
Hly3B2-20	60 g of HNTs +40 ml of a solution with a boron concentration of 20 %
Hly3B2-05	60 g of HNTs +40 ml of a solution with a boron concentration of 5 %
Hly60I40	60 g of HNTs +40 ml of an iodine solution
Hly80I20	80 g of HNTs +20 ml of an iodine solution
Hly95I05	95 g of HNTs +5 ml of an iodine solution

Note: In the sample code Hly3Cu2-40, "Hly3" corresponds to the halloysite weight used (e.g., 60 g), and "Cu2" reflects the molar ratio of halloysite to copper solution (3:2). The number "40" indicates the concentration of copper chelated in the solution. This nomenclature is applied consistently to all nanocomposite labels in this study.

2.3. Characterization of the nanocomposites

To investigate parameters of the produced nanocomposites and verify sorption of (Cu, B, I) into halloysite nanotube structures, a range of laboratory and analytical investigations were conducted, which included scanning electron microscopy with energy dispersive X-ray spectroscopy (SEM-EDX), Brunauer-Emmett-Teller (BET), transmission electron microscopy (TEM) with selected area electron diffraction (SAED), Fourier transform infrared spectroscopy (FTIR), X-ray diffraction analysis (XRD), thermogravimetric and differential scanning calorimetry with mass spectrometry (TG-DSC-MS), and inductively coupled plasma mass spectrometry (ICP-MS).

Scanning electron microscopy (SEM) was used to analyze the nanocomposite morphological features and chemical composition. The study was conducted with a TESCAN Vega 3 SBU scanning electron microscope (TESCAN, Brno, Czech Republic) that is equipped with an OXFORD X-Max 50 energy-dispersive X-ray spectroscopy detector (Oxford Instruments, Abingdon, UK). The imaging conditions included an accelerating voltage of 10–20 kV, a 3–12 nA sample current, a 5–15 mm working distance, and operation under full vacuum mode. The samples examined comprised dried, powder-like nanocomposites alongside raw halloysite material. Outer diameters of halloysite nanotubes were statistically analyzed from SEM images with over 150 measurements per sample used to construct diameter distribution histograms. Additionally, plant leaves treated with aqueous nanocomposite solutions were analyzed to assess interactions between the plant tissues and halloysite nanotubes.

The specific surface area of the nanocomposites was determined using the Brunauer-Emmett-Teller (BET) method with a 3P sync 210 surface area and porosity analyzer (Ribori Instrumentation, Germany). Before analysis, the samples were pre-dried at 125 °C for 2 h and then degassed under vacuum at 250 °C for 12 h. Surface area measurements were conducted at −196 °C over a relative pressure range 0.05–0.3. Nitrogen adsorption-desorption isotherms were also utilized to determine the total pore volume and average pore size. Pore size distributions were calculated using the Barrett-Joyner-Halenda (BJH) method. Representative pore size distribution curves are provided in the Supplementary information (Fig. S1).

Transmission electron microscopy (TEM) was employed to investigate the structural organization of halloysite nanotubes before and after chemical modification and assess the localization of Cu, B, and I within the nanotube lumen. Imaging was performed using a JEOL JEM-2100F microscope (JEOL, Tokyo, Japan) operating at 200 kV. Sample preparation involved finely grinding the nanocomposites and then dispersing them onto a copper grid coated with a carbon film. The TEM images, supplemented by selected area electron diffraction (SAED), facilitated the evaluation of structural transformations in the nanocomposites.

Fourier transform infrared (FTIR) spectroscopy was used to identify the nanocomposites' chemical bonds and functional groups. Spectra were recorded using a Shimadzu FTIR 8400S spectrometer (Kyoto, Japan) over a wavenumber range of 4000-400 cm^{-1}. Using the KBr pellet technique ensured a resolution of 4 cm^{-1}, enabling a detailed characterization of the functional groups and molecular interactions within the nanocomposites.

X-ray diffraction (XRD) analysis was conducted to determine the crystal characteristics of the initial halloysite sample and the synthesized nanocomposites, as well as to assess the interlayer spacing within halloysite crystals. The measurements were performed using a Rigaku Ultima IV diffractometer equipped with a Cu Kα radiation source, operating at 40 kV and 30 mA. Diffraction patterns were collected from 3° to 65° on a 2θ scale at a scanning speed of 1° per minute, with a step interval of 0.02°.

Thermogravimetric and differential scanning calorimetry (TG-DSC) analyses were performed on the synthesized nanocomposites within a temperature range of 30–1000 °C under an inert argon atmosphere, using a controlled heating rate of 10 °C/min. The experiments were carried out on an STA 449 F5 Jupiter thermal analyzer (NETZSCH, Germany). To simultaneously identify evolved gas species, TG-DSC measurements were integrated with a Netzsch TA Quadrupole Mass Spectrometer (QMS) 403C Aeolos via a transfer line maintained at 250 °C. The mass spectrometer operated in electron impact ionization mode, analyzing mass-to-charge (m/z) ratios from 1 to 50.

The elemental contents were measured using inductively coupled plasma mass spectrometry (ICP-MS) on an ELAN DRC-e mass spectrometer. The analyzed samples, weighing 0.5 g, were melted at 1050 °C with a mixture of lithium metatetraborate ($LiBO_2/Li_2B_4O_7$) to eliminate acidic and alkaline oxides. After melting, the samples were placed in a glass-carbon crucible and heated for 6 h at 120 °C. During this time, a mixture of concentrated acids (HF, HNO_3, and $HClO_4$) in a ratio of 5:4:1.5 was added to dissolve the glass formations. The mass was evaporated at 160 °C to obtain wet salts using 10 ml of 5 M HNO_3 solution. After these steps, the solutions were filtered, and the elements were analyzed.

2.4. Plant growth tests

An experiment was conducted on arugula microgreens (*Eruca sativa*) to evaluate the effectiveness of nanocomposites. Four microgreen trays were used in the study, which were treated using nanocomposites with copper (Hly3Cu2-40), boron (Hly3B2-40), iodine (Hly60I40), and a complex nanocomposite containing all three elements. The control sample was grown without fertilizer application.

The microgreens were grown in four plastic trays under controlled conditions (temperature 24.5 °C, humidity 64 %). Each tray was divided into sections corresponding to one treatment group.

Aqueous suspensions were prepared at a ratio of 0.1 g of nanocomposite per 50 ml of water and applied by foliar spraying three times during the experiment. The experiment lasted 14 days, during which seed germination rate, plant height, and biomass weight were measured.

To simulate natural conditions, plants were rinsed with distilled water at regular intervals. Statistical analysis was performed using Student's t-test ($p < 0.05$) to assess differences in plant growth parameters.

3. Results

3.1. Nanocomposite morphology

The initial HNTs concentrate consists of randomly oriented nanotubes, each measuring less than 5 μm in length and approximately 95 nm in average outer diameter (Fig. 1 A). A morphometric analysis using scanning electron microscopy (SEM) images was conducted to study the morphological changes of halloysite nanotubes following activation (Table 2). The initial nanotube width ranged from 40 to 162 nm (Fig. 1 A).

After chemical activation (Fig. 1B–D), the average nanotube outer diameter increased to 125–184 nm, with the maximum observed outer

Table 2
Outer diameters of loaded HNTs.

Nanocomposites	Outer diameter, nm		
	Minimum	Average	Maximum
Original HNTs	40	96	162
Hly3Cu2-05	72	125	220
Hly3Cu2-20	120	183	280
Hly3Cu2-40	93	136	268
Hly3B2-05	92	164	267
Hly3B2-20	119	184	288
Hly3B2-40	93	165	303
Hly95I-05	92	164	267
Hly80I-20	110	175	288
Hly60I-40	72	125	220

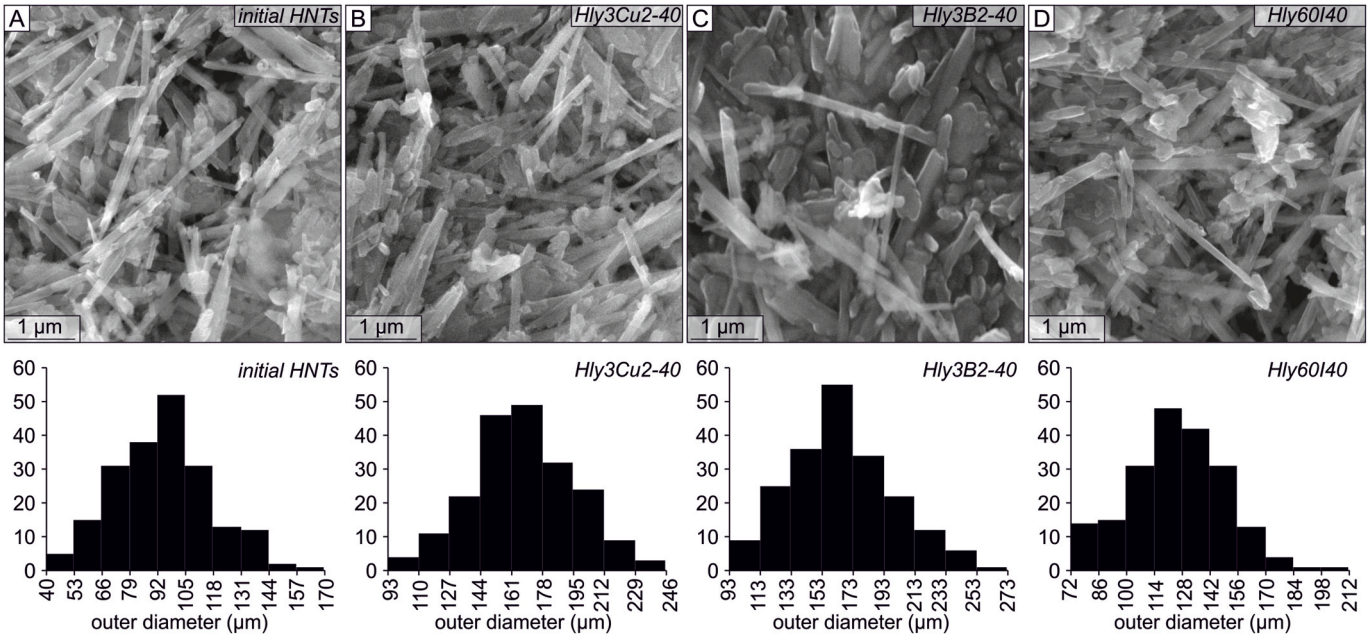

Fig. 1. SEM images obtained using a secondary electron detector (top) and histograms distribution of outer diameter distributions (bottom) of the original HNTs (A) and nanocomposites activated with chelated copper, acidic boron, and iodine solutions: (B) Hly3Cu2-40, (C) Hly3B2-40, (D) Hly60I40.

diameter reaching 270 nm in the Hly3B2-40 nanocomposite (Fig. 1 C). These findings confirm the morphological transformations of HNTs induced by chemical modification.

The specific surface area of nanocomposites varies based on the components and their concentrations (Table 3). The initial surface area of the halloysite is 20.2 m^2/g. Adding copper chelate reduces the surface area, particularly in the Hly3Cu2-40 sample, which measures 18.5 m^2/g (an 8.4 % decrease) due to pore filling with copper particles. In contrast, due to surface activation at a lower copper concentration (Hly3Cu2-05), the surface area increases by 10.9 %–22.4 m^2/g. For Hly3B2-40, boric acid's impact on the pore structure decreases surface area by 6.4 %, while Hly3B2-05 shows a 5 % increase in surface area relative to halloysite, indicating improved pore distribution at lower concentrations. Iodine has a mixed effect; Hly60I40 shows the highest surface area at 23.3 m^2/g (a 15.3 % increase) due to enhanced adsorption related to its hygroscopic properties. Even at lower iodine concentrations, like Hly95I05 (22.3 m^2/g), the surface area remains above that of halloysite, showing a 10.4 % increase.

The total pore volume for nanocomposites (Table 3) remains stable at 0.1 cm^3/g, except for the Hly60I40 sample, which slightly increases to 0.12 cm^3/g. This suggests that iodine modification enhances the total pore volume by preserving the existing porous structures.

The average pore size experiences minimal variation (Table 3). The original halloysite has an average pore size of 18.6 nm. However, increasing concentrations of copper, boron, or iodine increase the pore size, reaching a maximum of 21.8 nm in the Hly3Cu2-40 sample. Lower concentrations of copper and boron additives help maintain the pore size within the 18.4–18.6 nm range. The BJH pore size distribution curves derived from the desorption branch (Fig. S1) revealed a significant shift toward larger mesopores upon chemical activation. Compared to initial halloysite nanotubes, the modified samples exhibit broader distributions with increased pore volumes in the 2–20 nm range, indicating the partial dissolution of aluminosilicate walls and the formation of secondary mesoporosity. Among the studied nanocomposites, Hly3Cu2-40 showed the most pronounced shift in the average pore diameter and volume, suggesting that copper chelate treatment was the most effective in restructuring the tubular wall architecture.

A noticeable increase in interlayer distances was observed in the TEM-SAED analysis. The thickness of the crystal unit structure increases from 7.2 Å to 7.8 Å as the concentration of the solution rises due to the formation of complexes on the basal crystal plane of the halloysite. This change is particularly evident in the Hly3B2-40 and Hly3Cu2-40 composites (Fig. 2), which demonstrate enhanced interlayer spacing. The TEM SAED patterns confirm the results from the XRD, highlighting structural changes in the nanocomposites. The interlayer distances and crystal packet thickness variations indicate enhanced properties associated with interactions at different solution concentrations.

Table 3
Specific surface area, total pore volume, and average pore size in halloysite nanocomposites BET analysis.

Nanocomposites	Specific surface area (m^2/g)	Total pore volume (cm^3/g)	Average pore diameter (nm)
Hly3Cu2-40	18.5	0.10	21.8
Hly3Cu2-20	19.3	0.10	21.0
Hly3Cu2-05	22.4	0.10	17.3
Hly3B2-40	18.9	0.10	21.4
Hly3B2-20	20.8	0.10	18.6
Hly3B2-05	21.2	0.10	18.4
Hly60I40	23.3	0.12	21.1
Hly80I20	21.9	0.10	18.8
Hly95I05	22.3	0.10	18.4
original halloysite	20.2	0.10	18.6

3.2. Structural characteristics of nanocomposites

FTIR was conducted to examine the chemical interactions occurring in halloysite nanocomposites after modification with Cu, B, and I (Fig. 3). The FTIR spectra of pristine halloysite and modified samples are shown in Fig. 3. For the pure halloysite, characteristic absorption bands were observed at 3694 cm^{-1} and 3620 cm^{-1}, corresponding to the stretching vibrations of OH hydroxyl groups. The band at 1031 cm^{-1} is assigned to the *Si*-O stretching vibrations in the tetrahedral layer. The *Si*-O-Al linkages and Al-OH bending vibrations are detected within 400–950 cm^{-1}, confirming the layered silicate structure of halloysite. Upon chemical activation, notable shifts and intensity variations were observed in the spectra. New band emerged at 1400 cm^{-1}, which can be attributed to Cu-O stretching vibrations. For iodine-loaded nanocomposites, new peaks appeared at 870 cm^{-1}, corresponding to I-O interactions.

The X-ray diffraction (XRD) pattern of the original halloysite (Fig. 4) shows characteristic basal reflections corresponding to halloysite, kaolinite, feldspar, and quartz. A very weak reflection at 10.1 Å suggests the predominance of dehydrated halloysite (7 Å), with a minor fraction of interlayer water molecules forming a hydrated 1:1 packet. Specific reflections at 10.3–10.5, 7.2, 5.1, 4.5, 4.1, and 3.7 Å are attributed to modified halloysite (7 Å and 10 Å) and kaolinite.

After activation with chelated copper, boron acid, and iodine, significant structural changes are observed in the nanocomposite diffractograms, particularly a prominent basal reflection at 10.3–10.5 Å (Fig. 4). The most considerable interplanar distance (001) is recorded in the Hly3Cu2-20 and Hly3Cu2-40 nanocomposites, reaching 10.5 Å. The shift in the primary basal reflection and its enhanced intensity indicates the intercalation of water and added ions into the halloysite 1:1 interlayer space, increasing the interplanar distance by 3.2 Å. The basal reflection at 7.2 Å remains unchanged across all nanocomposites, suggesting structural stability in this particular phase despite chemical activation.

3.3. Chemical composition of nanocomposites

Differential scanning calorimetry (DSC) of the nanocomposites reveals several endothermic and exothermic effects (Fig. 5). The most significant endothermic peak occurs between 527 and 534 °C, corresponding to the dehydroxylation of structural water, specifically the decomposition of Al-OH hydroxyl groups. As the concentration of reactive solutions increases, particularly in Hly3Cu2-40 and Hly3B2-40, this endothermic effect shifts to higher temperatures. Additionally, a sharp exothermic peak is observed in the 970–998 °C range, whose position varies depending on the nanocomposite composition. This peak indicates the formation of new phases, including metakaolin and possibly other crystalline phases. The lowest temperature for this effect (970 °C) is characteristic of Hly3B2-40, while the highest temperature (998 °C) is observed in the original halloysite. For the endothermic peak (480–580 °C), which is associated with halloysite dehydroxylation and interlayer water loss, the highest ΔH values (Table S1) were recorded in low-loading composites such as Hly3Cu2-05 (20.1 kJ/g) and Hly3B2-05 (20.4 kJ/g), while raw HNTs showed a considerably lower enthalpy (7.5 kJ/g). The exothermic enthalpy (970–998 °C) decreased significantly after chemical activation, indicating progressive removal or transformation of reactive surface species.

Thermogravimetric (TG) analysis of the nanocomposites reveals four distinct weight loss intervals (Fig. 5, Table S2): 30–160 °C, 160–410 °C, 410–570 °C, 570–1000 °C. In the first temperature range (30–160 °C), the primary mass loss is associated with the removal of physically adsorbed water. Mass loss varies from 0.2 % in Hly3Cu2-05 to 3.3 % in Hly60I40. Iodine-modified nanocomposites show the highest mass loss because of their significant hygroscopicity, which increases water adsorption. This observation is supported by mass spectrometry analysis, which detected ion currents corresponding to H_2O, CH_3^+, CO_2, and

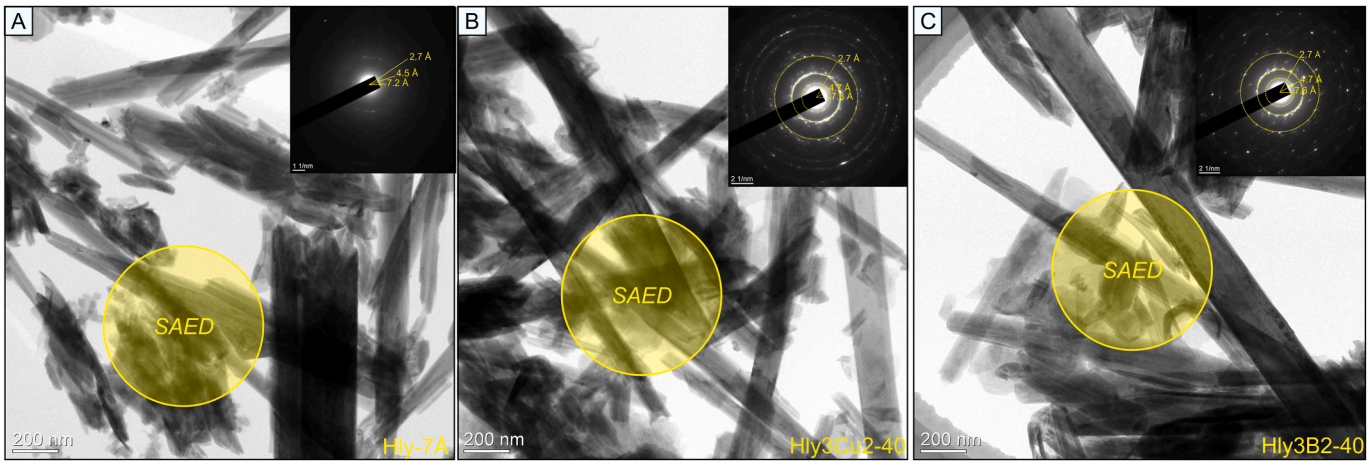

Fig. 2. TEM images with selected area electron diffraction patterns (yellow circle) of original halloysite (A) and those activated by chelated copper and acidic boron solutions: (B) Hly3Cu2-40, (C) Hly3B2-40.

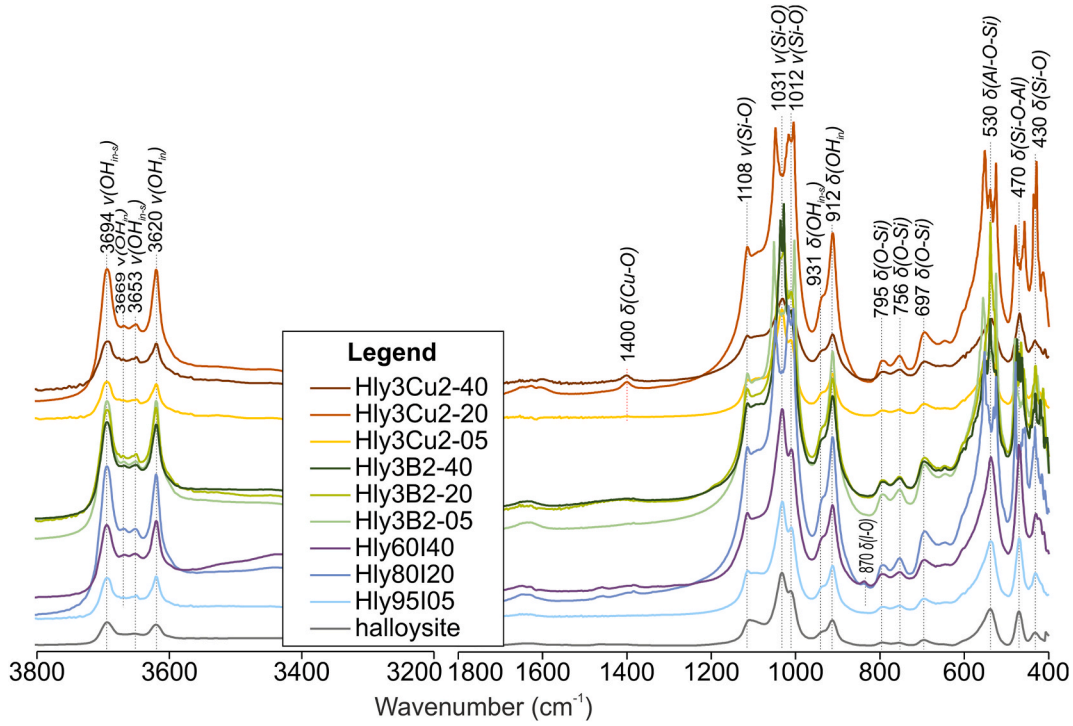

Fig. 3. FTIR spectra of the original halloysite and activated nanocomposites.

other volatile compounds (Fig. 6 C). In contrast, the lowest mass loss values are found in samples with minimal additive concentrations, such as Hly3Cu2-05, suggesting either a denser microstructure or a reduced number of available adsorption sites for water molecules.

Between 160 and 410 °C, both mesoporous and interlayer water are gradually removed from the samples. The recorded mass loss ranges from 1.0 % in Hly3B2-02 to 2.3 % in Hly3Cu2-40. The highest mass loss is observed in the copper-modified nanocomposites, likely due to their impact on the halloysite structure, which promotes the release of a greater fraction of interlayer water. A distinctive feature of copper-containing nanocomposites is the pronounced release of decomposition products from chelate complexes, particularly CH_2O^+ ions (Fig. 6 A). In contrast, boron-modified nanocomposites exhibit minimal mass loss, suggesting a potential stabilizing effect of boron on the interlayer structure. B-containing ions, including BO^+ species, are also detected in these nanocomposites (Fig. 6 B). A non-linear trend was observed in the B-loaded series, with Hly3B2-20 showing slightly lower loading than Hly3B2-05. This may be related to the solubility and coordination behavior of boric acid at intermediate concentrations, leading to partial desorption during drying.

The most significant mass losses occur in the temperature range of 410–570 °C, corresponding to the dehydroxylation of the halloysite crystal lattice. Within this range, mass loss varies from 8.3 % in Hly3B2-40 to 9.1 % in Hly3Cu2-40. Copper-modified nanocomposites exhibit the highest mass loss, likely due to the strong interaction between copper chelate ions and hydroxyl groups in the halloysite structure. Mass spectrometry confirms the presence of decomposition products, including SO^+ and CH_2O^+ ions (Fig. 6 A). In contrast, boron addition appears to stabilize the structure, reducing mass loss within this temperature interval, as indicated by the lower values recorded for boron-modified nanocomposites.

In the temperature range of 570–1000 °C, which corresponds to the

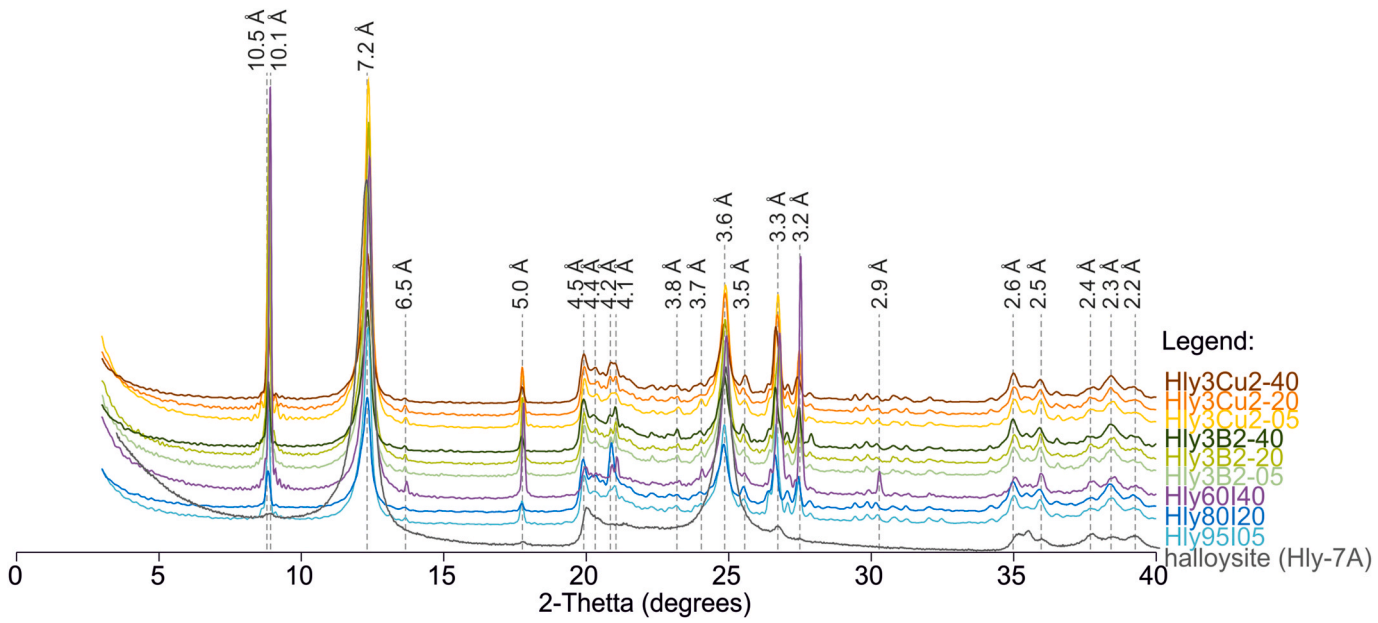

Fig. 4. XRD patterns of the original halloysite (Hly-7Å) and activated nanocomposites.

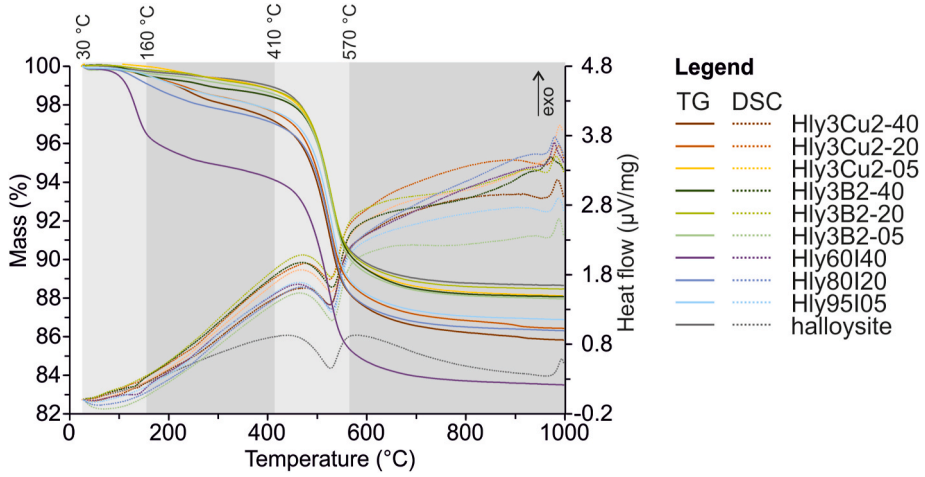

Fig. 5. Thermogravimetric (TG) and differential scanning calorimetry (DSC) curves for the original halloysite and the nanocomposites.

final removal of hydroxyl groups and structural transformations, mass loss varies from 1.7 % in Hly60I40 to 2.3 % in Hly3Cu2-40. The highest mass loss in this range is observed in copper-modified nanocomposites, likely due to the interaction of copper with the residual halloysite structure and the potential partial formation of new phases. A peak corresponding to SO^{+} ions is also detected (Fig. 6 A). In contrast, iodine-modified nanocomposites exhibit minimal mass loss, suggesting that the main degradation processes were completed at earlier stages.

ICP-MS analysis demonstrated that the chemical composition of halloysite nanocomposites undergoes several interrelated changes depending on the concentration of active additives. The copper content in Cu-modified nanocomposites increases from 298 ppm in Hly3Cu2-05 to 2051 ppm in Hly3Cu2-40, confirming the successful incorporation of copper into the mineral structure. Similarly, sodium levels increase from 0.08 % to 0.22 % in these nanocomposites, likely due to its role as an inert component in the diffusion of exchangeable ions. In contrast, the aluminum content decreases with increasing additive concentration, dropping from 18.0 % in Hly3Cu2-05 to 9.8 % in Hly3Cu2-40. This reduction suggests that highly concentrated solutions facilitate aluminum removal during chemical activation. The high copper content in Hly3Cu2-40 further supports its intercalation into the halloysite structure.

3.4. Interaction of nanotubes with the plant surface and influence on the plant growth

Applying the nanocomposite to the surface of leaves (*Eruca sativa*) resulted in a uniform distribution, forming a pattern that corresponds to the circular morphology of the leaves (Fig. 7A). As illustrated in Fig. 7B, halloysite nanotubes were evenly distributed across the leaf surface. High-magnification SEM images (Fig. 7B–C) revealed that the nanotubes were adsorbed and physically embedded into the cuticle and stomatal openings of the leaf epidermis. The needle-like morphology of the halloysite enabled localized mechanical penetration, suggesting an injection-like mode of interaction with the plant tissue. The microstructural interaction between the nanotubes and the leaf surface occurs through a combination of adsorption and penetration mechanisms. The nanocomposites demonstrated strong adhesion to the plant leaves when simulating airflow conditions by blowing compressed air. This localized retention of nanotubes suggests their stable integration into the leaf

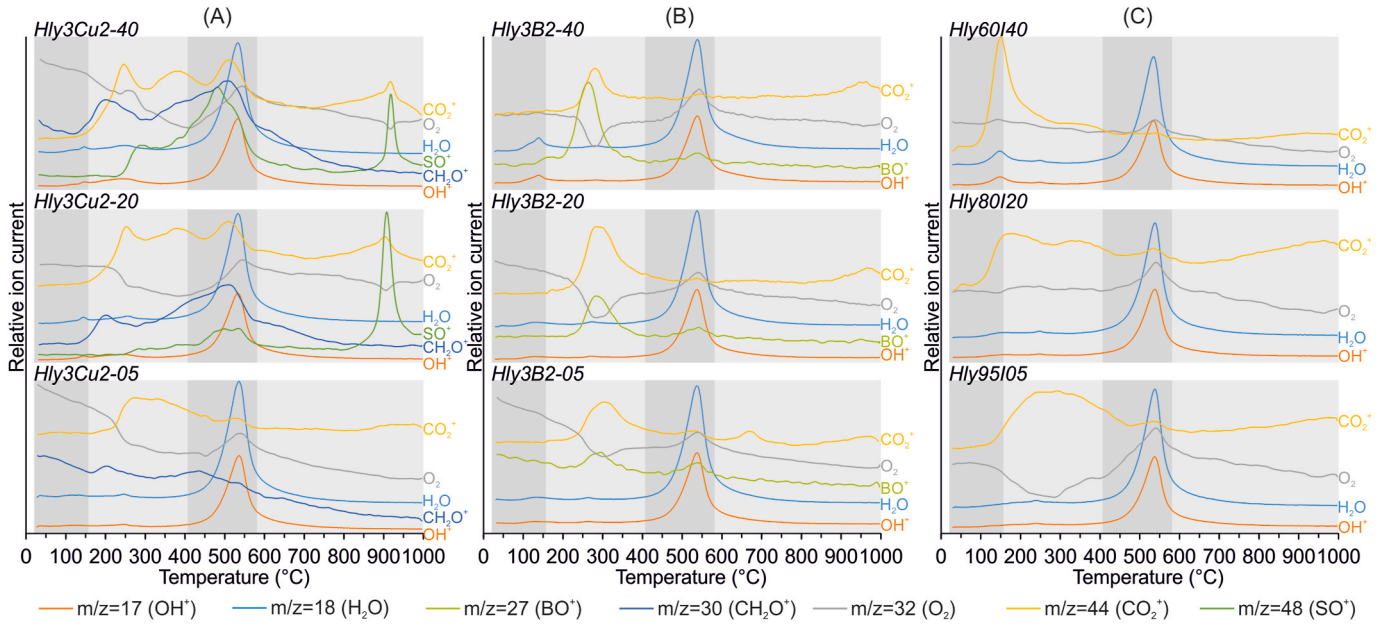

Fig. 6. Selected representative mass spectrometry (MS) curves for nanocomposites, showing ion signals corresponding to mass-to-charge ratios (*m/z*): 17 (OH^+), 18 (H_2O), 27 (BO^+), 30 (CH_2O^+), 32 (O_2), 44 (CO_2) и 48 (SO^+).

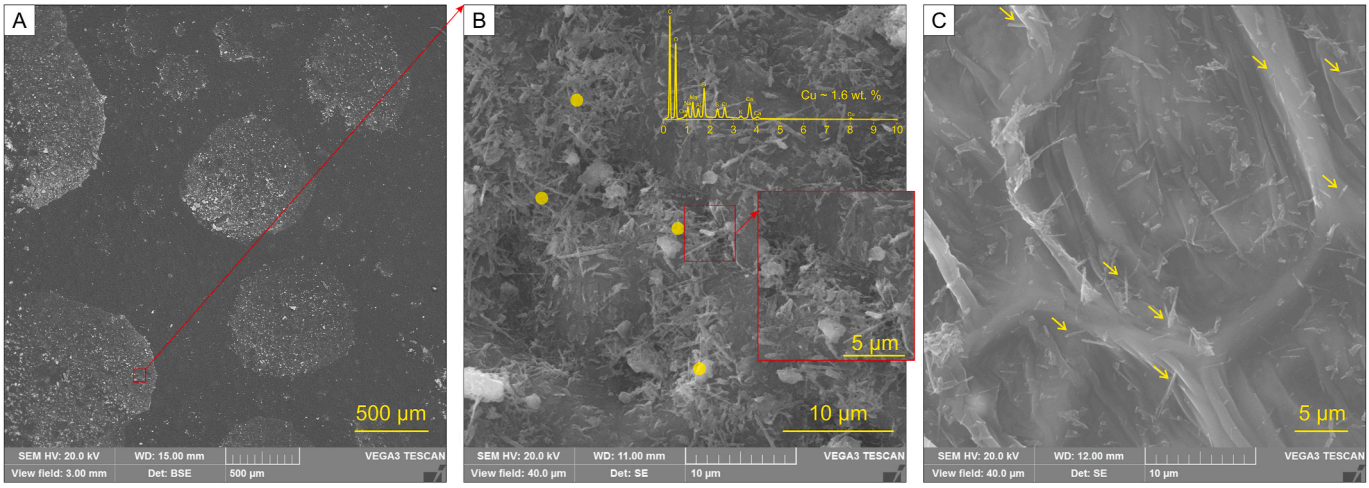

Fig. 7. SEM images showing the interaction of halloysite nanotubes with the surface of plant tissue (*Eruca sativa*). (A) Uniform distribution of nanocomposites on the leaf epidermis, matching its circular surface morphology. (B) Widespread and dense coverage of the plant surface by halloysite nanotubes. A representative EDX spectrum (in yellow circles) confirms the elemental distribution of copper within nanotube-treated zones. (C) High-magnification image demonstrating the physical penetration ("injection") of individual nanotubes into stomatal openings and cuticular tissue, as highlighted by yellow arrows.

structure. EDS analysis revealed that copper (Cu) is homogeneously distributed across the regions covered by nanotubes, with Cu content ranging from 0.7 % to 1.9 % and an average of approximately 1.6 %.

The results of the experiment showed that boron-containing nanocomposites and the complex nanocomposite had the most pronounced effect on plant height, leading to an 84 % increase in growth (Figs. 8 and 9 A). The Cu-modified nanocomposite (Fig. 9 B) resulted in the most significant increase in plant biomass, with an increase of 3.8 g (42 %) compared to the control. The complex nanocomposite ranked second in effectiveness, increasing plant weight by 3.1 g (34 %).

Plants treated with the Cu-containing nanocomposite exhibited the highest dry weight after water removal, followed by the complex nanocomposite (Figs. 8 and 9 C). The dry weight increase across all fertilizer-treated samples was consistent but significantly higher than that of the control, ranging from 26 % to 35 %.

4. Discussion

4.1. Halloysite nanotubes as tunable carriers for micronutrient (Cu/B/I) delivery

The advancement of nanotechnology has led to the development of fertilizers at the nanoscale, which improves nutrient absorption and reduces environmental harm [50]. Layered minerals are essential in formulating nano-fertilizers due to their excellent ion exchange capacity, adsorption properties, and ability to regulate nutrient release [51]. Halloysite nanotubes (HNTs) have gained significant attention as promising nanocarriers for targeted nutrient delivery [52–54]. Their distinctive hollow tubular morphology, high specific surface area, and capacity to encapsulate active compounds make them ideal for controlled-release fertilizers. Previous studies have demonstrated the successful intercalation of essential micronutrients, such as zinc, into

Fig. 8. Microgreens (*Eruca sativa*) at the start (A) and end (B) of the experiment, with sprout growth labelled. Note: all – complex composite, B – Hly3B2-40, Ct – control sample, Cu – Hly3Cu2-40, I – Hly60I40.

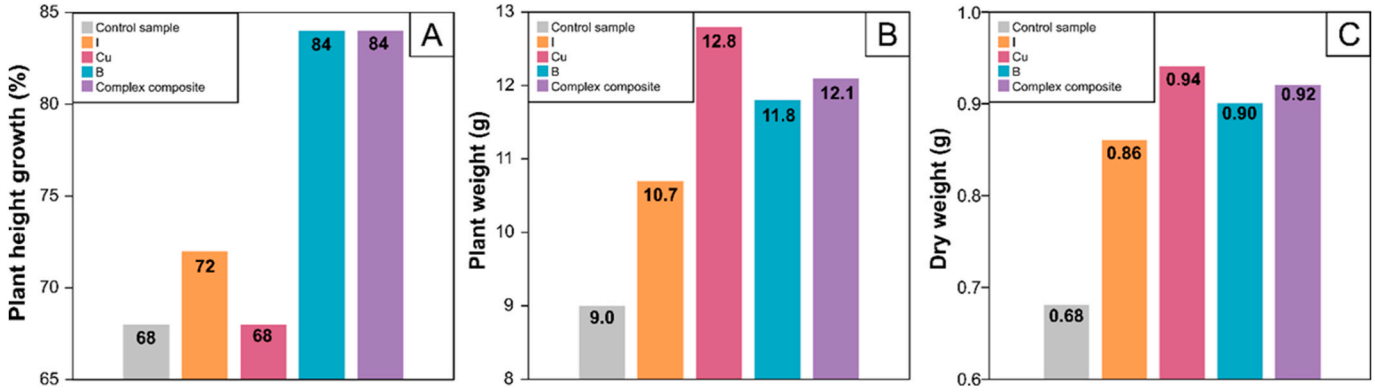

Fig. 9. Histograms showing the distribution of primary growth parameters of arugula microgreens (*Eruca sativa*). Note: B – Hly3B2-40, Cu – Hly3Cu2-40, I – Hly60I40.

halloysite for agricultural applications [55–57]. The potential of halloysite-based nanocomposites modified with other micronutrients, such as copper, boron, and iodine, remains insufficiently explored.

The modification of HNTs with Cu, B, and I also induces significant morphological changes (Fig. 1). The nanotube outer diameter increased from 96 nm (initial halloysite) to 165 nm (Hly3B2-40), with maximum observed values reaching up to 270 nm (Table 2). These changes suggest structural reorganization associated with incorporating additives into the macro- and mesoporous spaces of halloysite.

At high concentrations, both copper and boron reduce the specific surface area of mineral materials. Copper fills the pores, while boron interacts with the porous framework. At lower concentrations, copper enhances the surface area by altering the structure, whereas boron's effect is minimal. In contrast, iodine (especially at higher concentrations) improves both the specific surface area and total pore volume by attracting moisture and increasing nitrogen adsorption. Despite these changes, the average pore size remains consistent, indicating that the halloysite structure remains unaltered. The BJH desorption analysis further substantiated these findings, indicating that the Cu- and B-modified samples, particularly Hly3Cu2-40, demonstrated a significant shift in pore volume distribution toward the mesoporous range of 2–20 nm. The analysis revealed defined peaks around 4–6 nm (Fig. S1). This shift indicates a partial restructuring of the aluminosilicate framework and accessibility of internal channels. This stability is crucial for potential applications in catalysis, adsorption, and controlled release systems.

FTIR spectra revealed characteristic shifts in vibrational bands (Fig. 3), including new Cu-O stretching vibrations at 1400 cm^{-1} and I-O interactions at 870 cm^{-1}, confirming the successful incorporation of these elements in HNTs. A shift in the primary basal reflection from 10.1 Å to 10.3–10.5 Å (Fig. 4), particularly in Hly3Cu2-20 and Hly3Cu2-40, indicating that water and metal ions intercalated into the halloysite interlayer space (Fig. 2). The basal reflection at 7.2 Å remained unchanged across all nanocomposites, suggesting the stability of halloysite crystal layers despite chemical activation.

Copper content increased from 298 ppm in Hly3Cu2-05 to 2051 ppm in Hly3Cu2-40 (Table 4), confirming its incorporation into the halloysite framework. Sodium concentrations also increased slightly from 0.08 % to 0.22 %, possibly linked to its role in ion exchange. In contrast, aluminum content decreased from 18.0 % (Hly3Cu2-05) to 9.8 % (Hly3Cu2-40), suggesting that aluminum removal or substitution occurs during high-concentration chemical activation. Similar stabilization effects were observed for boron-modified nanocomposites.

This study shows that the micronutrient substances influence the thermal characteristics of halloysite nanocomposites. I-ions enhance water absorption and release at lower temperatures, allowing for controlled ion transfer. Cu-ions accelerate the mass loss and degradation of the material within the temperature range of 410–570 °C. B-ions strengthen the composite, resulting in reduced mass loss and improved structural integrity. The increase in endothermic enthalpy after chemical loading reflects enhanced water retention and surface coordination, particularly in samples with lower nutrient concentrations. This suggests a more hydrated and structurally dynamic halloysite matrix. In contrast, the reduction of the high-temperature exothermic enthalpy (from 3.0 kJ/g in initial HNTs to <1.2 kJ/g in nanocomposites) implies effective depletion of new phases, possibly introduced during chelation or acid treatment.

Table 4
Elemental composition of halloysite nanocomposites (excluding iodine-containing samples) based on ICP-MS analysis.

Nanocomposites	Na (%)	Mg (%)	Al (%)	K (%)	Fe (%)	Cu (ppm)	As (ppm)
Hly3Cu2-40	0.22	0.06	9.80	2.32	0.95	2051.1	19.4
Hly3Cu2-20	0.18	0.06	12.02	2.32	0.97	1363.7	19.1
Hly3Cu2-05	0.08	0.08	17.96	2.41	0.96	298.2	20.7
Hly3B2-40	0.06	0.07	12.80	2.34	0.94	36.6	18.4
Hly3B2-20	0.06	0.07	15.61	2.22	0.95	36.5	20.6
Hly3B2-05	0.05	0.06	12.52	2.14	0.92	41.5	18.5

These properties suggest that tailored chemical activation of halloysite nanotubes enables the design of nanocomposites with controlled release properties suitable for agricultural and environmental applications.

Compared to previously reported nanocomposites based on halloysite modified with a single nutrient element (e.g., Zn [57]), the current study introduces a multifunctional halloysite platform capable of simultaneously incorporating Cu, B, and I. In contrast to earlier Zn/Cu/B glauconite-based systems with globular morphology [58] and limited penetration potential, developed HNT-based nanocarriers exhibit tunable tubular morphology, high surface activity, and a unique ability to anchor to physically and even penetrate plant epidermis, as shown in Fig. 7 C. Furthermore, unlike other advanced formulations relying on synthetic coatings or pesticide loading [53], our system remains fully mineral-based and biocompatible, offering environmentally sustainable micronutrient delivery. The multifunctionality, injectable behavior, and surface adhesion capacity of Cu/B/I-loaded halloysite nanocomposites provide a distinct advantage in designing smart agro-inputs for foliar applications.

4.2. Growth enhancement and nutrient efficiency of Cu/B/I-loaded halloysite nanocomposites

The application of Cu/B/I-modified halloysite nanocomposites led to their uniform distribution on the surface of plant leaves, forming a pattern that corresponded to the natural circular morphology of the leaf epidermis (Fig. 7 A). As shown in Fig. 7B, the nanotubes were uniformly dispersed and exhibited clear interaction with the leaf surface via adsorption and physical penetration. This penetration effect, called "injectable action," supports their strong affinity to the plant epidermis. Tests under simulated wind conditions (compressed air flow) confirmed strong adhesion of the nanotubes to the leaf surface. EDX analysis indicates a uniform distribution of copper in the treated areas.

After a two-week application of the nanocomposites, significant growth of arugula (*Eruca sativa*) enhancements were observed. The boron-containing nanocomposites and the complex Cu/B/I nanocomposite had the most pronounced effect on plant height, increasing growth by 84 % compared to the control (Figs. 8 and 9 A). Meanwhile, the Cu-modified nanocomposite exhibited the highest increase in plant biomass, with a total weight increase of 42 % relative to untreated plants (Fig. 9 B). The complex nanocomposite ranked second in effectiveness, increasing plant biomass by 34 %.

The evaluation of dry weight after water removal further confirmed the effectiveness of the Cu-containing nanocomposites, which demonstrated the highest dry weight retention, followed by the complex nanocomposite (Figs. 8 and 9 C). Across all samples treated with fertilizers, the dry weight gain was consistently higher than that of the control, ranging from 26 % to 35 %.

This results are consistent with previous reports demonstrating that functionalized halloysite nanotubes act as efficient carriers for nutrient delivery, particularly through foliar pathways. For example, halloysite nanotubes functionalized with chitosan have been shown to penetrate root tissues and accumulate within the epidermal and endodermal layers, leading to enhanced nutrient absorption [59,60]. Similarly, slow-release fertilizers incorporating halloysite nanotubes into biodegradable starch matrices have exhibited prolonged nutrient availability and reduced leaching losses [52,61]. In contrast to earlier systems, the Cu/B/I-loaded halloysite nanocomposites offer stable surface adhesion and nutrient delivery in a single action.

A key advantage of our approach is the simultaneous incorporation of different micronutrients into a single nanocarrier system. While previous studies have focused primarily on Zn-modifications of halloysite for controlled release [57], our results demonstrate the potential for

other elements to enhance plant development comprehensively due to targeted option of nanofertilizers.

Despite these promising results, further research is needed to assess long-term effects and potential phytotoxicity at higher dosages. Previous studies have reported that halloysite nanotubes may exhibit inhibitory effects on plant germination at concentrations exceeding 50 mg/ml, particularly in *Brassica Rapa* L. and *Cynodon Dactylon* [62]. Our findings suggest that Cu/B/I nanocomposites effectively promote plant growth within the tested concentration range.

This study underscores the potential of Cu/B/I-modified halloysite nanotubes as multifunctional carriers for micronutrient delivery with the injectable action, enhancing plant growth while ensuring controlled nutrient release. By integrating micronutrient delivery with sustainable nanotechnology, these nanocomposites offer a promising strategy for precision agriculture and optimized fertilizer formulations.

5. Conclusions

This study presents a novel approach to developing Cu/B/I-modified halloysite-based nanofertilizers with targeted nutrient delivery properties.

(1) The chemical modification of halloysite using Cu, B, and I-containing solutions resulted in efficient incorporation of micronutrients through surface adsorption and partial intercalation. The modification of halloysite nanotubes induced significant morphological changes, including an increase in nanotube outer diameter from 96 nm (initial halloysite) to 165 nm (Hly3B2-40), with maximum observed values reaching up to 270 nm. These transformations confirm that Cu, B, and I are incorporated within the mesopores and micropores of the halloysite.
(2) A shift in the primary basal reflection from 10.1 Å to 10.3–10.5 Å, particularly in Cu-modified samples (Hly3Cu2-20 and Hly3Cu2-40), indicates intercalation of water and metal ions into the interlayer space of halloysite. The basal reflection at 7.2 Å remained unchanged, suggesting the retention of the mineral 1:1 crystal layer despite chemical activation.
(3) The application of Cu/B/I nanocomposites to plant leaves resulted in a uniform distribution of nanotubes, with stable adhesion confirmed under simulated airflow conditions. EDX analysis revealed homogeneous Cu distribution across the treated leaf surface, supporting the potential of these nanofertilizers for foliar application.
(4) Growth experiments on arugula (*Eruca sativa*) demonstrated that copper/boron/iodine (Cu/B/I) nanocomposites significantly promote plant growth. Nanocomposites containing boron resulted in an 84 % increased plant height, while those modified with copper led to a 42 % enhancement in biomass. The treated plants exhibited dry weights 26 %–35 % greater than the control. This underscores the potential of halloysite-based nanofertilizers to enhance crop yield and nutrient use efficiency.
(5) Halloysite nanotubes were treated with copper, boron, and iodine to produce stable and effective nanofertilizers that contain micronutrients. These nanocomposites bond effectively to plant surfaces, promoting longer retention and minimizing nutrient leaching, which is crucial for sustainable agricultural practices.

CRediT authorship contribution statement

Evan Dasi: Writing – review & editing, Writing – original draft, Visualization, Investigation. **Ivan Khitrin:** Writing – original draft, Visualization, Investigation. **Alexey Ruban:** Writing – original draft, Validation, Resources, Investigation, Formal analysis. **Prokopiy Maximov:** Writing – original draft, Visualization, Investigation. **Natalia Maximova:** Writing – original draft, Visualization, Investigation. **Peng Yuan:** Writing – review & editing, Validation, Methodology, Formal analysis. **Maxim Rudmin:** Writing – review & editing, Writing – original draft, Visualization, Validation, Supervision, Resources, Project administration, Methodology, Investigation, Funding acquisition, Conceptualization.

Declaration of competing interest

The authors declare that they have no known competing financial interests or personal relationships that could have appeared to influence the work reported in this paper.

Acknowledgments

The authors gratefully acknowledge the financial support provided by the project FSWW-2023-0010. M.R. thanks Mikhail Kanin (Director of LLC “Halloysite-Ural”) for the provided mineral material. The authors sincerely thank the two anonymous reviewers and editor for their valuable comments and constructive feedback, which have greatly enhanced the quality and clarity of this manuscript.

Appendix A. Supplementary data

Supplementary data to this article can be found online at https://doi.org/10.1016/j.micromeso.2025.113663.

Data availability

Data will be made available on request.

References

[1] M.E. Trenkel, Controlled-Release and Stabilized Fertilizers in Agriculture, International Fertilizer Industry Association, Paris, France, 1997.
[2] C. Easwaran, S.R. Christopher, G. Moorthy, P. Mohan, R. Marimuthu, V. Koothan, S. Nallusamy, Nano hybrid fertilizers: a review on the state of the art in sustainable agriculture, Sci. Total Environ. 929 (2024) 172533, https://doi.org/10.1016/j.scitotenv.2024.172533.
[3] S. Moradi, A. Babapoor, S. Ghanbarlou, M.Y. Kalashgarani, I. Salahshoori, A. Seyfaee, Toward a new generation of fertilizers with the approach of controlled-release fertilizers: a review, J. Coating Technol. Res. (2023) 9–14, https://doi.org/10.1007/s11998-023-00817-z.
[4] J. Fu, C. Wang, X. Chen, Z. Huang, D. Chen, Classification research and types of slow controlled release fertilizers (SRFs) used - a review, Commun. Soil Sci. Plant Anal. 49 (2018) 2219–2230, https://doi.org/10.1080/00103624.2018.1499757.
[5] P. Vejan, T. Khadiran, R. Abdullah, N. Ahmad, Controlled release fertilizer: a review on developments, applications and potential in agriculture, J. Contr. Release 339 (2021) 321–334, https://doi.org/10.1016/J.JCONREL.2021.10.003.
[6] R. Chakraborty, A. Mukhopadhyay, S. Paul, S. Sarkar, R. Mukhopadhyay, Nanocomposite-based smart fertilizers: a boon to agricultural and environmental sustainability, Sci. Total Environ. 863 (2023) 160859, https://doi.org/10.1016/j.scitotenv.2022.160859.
[7] S. Govil, N. Van Duc Long, M. Escribà-Gelonch, V. Hessel, Controlled-release fertiliser: recent developments and perspectives, Ind. Crop. Prod. 219 (2024) 119160, https://doi.org/10.1016/J.INDCROP.2024.119160.
[8] C.O. Dimkpa, P.S. Bindraban, Nanofertilizers: new products for the industry? J. Agric. Food Chem. 66 (2018) 6462–6473, https://doi.org/10.1021/ACS.JAFC.7B02150/ASSET/IMAGES/MEDIUM/JF-2017-02150Z_0004.GIF.
[9] K.K. Verma, X.P. Song, A. Joshi, V.D. Rajput, M. Singh, A. Sharma, R.K. Singh, D. M. Li, J. Arora, T. Minkina, Y.R. Li, Nanofertilizer possibilities for healthy soil, water, and food in future: an overview, Front. Plant Sci. 13 (2022), https://doi.org/10.3389/fpls.2022.865048.
[10] P. Yuan, D. Tan, F. Annabi-Bergaya, Properties and applications of halloysite nanotubes: recent research advances and future prospects, Appl. Clay Sci. 112–113 (2015) 75–93, https://doi.org/10.1016/J.CLAY.2015.05.001.
[11] E. Abdullayev, Y. Lvov, Halloysite clay nanotubes for controlled release of protective agents, J. Nanosci. Nanotechnol. 11 (2011) 10007–10026, https://doi.org/10.1166/JNN.2011.5724.
[12] M. Massaro, G. Lazzara, R. Noto, S. Riela, Halloysite nanotubes: a green resource for materials and life sciences, Rendiconti Lincei 31 (2020) 213–221, https://doi.org/10.1007/S12210-020-00886-X/METRICS.
[13] M. Fahimizadeh, L.W. Wong, Z. Baifa, S. Sadjadi, S.A.B. Auckloo, K. Palaniandy, P. Pasbakhsh, J.B.L. Tan, R.K.R. Singh, P. Yuan, Halloysite clay nanotubes: innovative applications by smart systems, Appl. Clay Sci. 251 (2024) 107319, https://doi.org/10.1016/j.clay.2024.107319.
[14] E. Joussein, S. Petit, J. Churchman, B. Theng, D. Righi, B. Delvaux, Halloysite clay minerals — a review, Clay Miner. 40 (2005) 383–426, https://doi.org/10.1180/0009855054040180.

[15] R.F. Fakhrullin, M. Lvov, V.G. Mazurenko, Molecular dynamics of the halloysite nanotubes, Phys. Chem. Chem. Phys. 20 (2018), https://doi.org/10.1039/C7CP06575B.
[16] A.C. Santos, C. Ferreira, F. Veiga, A.J. Ribeiro, A. Panchal, Y. Lvov, A. Agarwal, Halloysite clay nanotubes for life sciences applications : from drug encapsulation to bioscaffold, Adv. Colloid Interface Sci. 257 (2018) 58–70, https://doi.org/10.1016/j.cis.2018.05.007.
[17] M. Liu, Z. Jia, D. Jia, C. Zhou, Recent advance in research on halloysite nanotubes-polymer nanocomposite, Prog. Polym. Sci. 39 (2014) 1498–1525, https://doi.org/10.1016/j.progpolymsci.2014.04.004.
[18] L. Yu, H. Wang, Y. Zhang, B. Zhang, J. Liu, Recent advances in halloysite nanotube derived composites for water treatment, Environ. Sci. Nano 3 (2016) 28–44, https://doi.org/10.1039/c5en00149h.
[19] Y. Zhang, H. Yang, Halloysite nanotubes coated with magnetic nanoparticles, Appl. Clay Sci. 56 (2012) 97–102, https://doi.org/10.1016/j.clay.2011.11.028.
[20] P. Yuan, D. Tan, F. Annabi-Bergaya, W. Yan, M. Fan, D. Liu, H. He, Changes in structure, morphology, porosity, and surface activity of mesoporous halloysite nanotubes under heating, Clays Clay Miner. 60 (2012) 561–573, https://doi.org/10.1346/CCMN.2012.0600602.
[21] G. Cavallaro, S. Milioto, G. Lazzara, Halloysite nanotubes: interfacial properties and applications in cultural heritage, Langmuir 36 (2020) 3677–3689, https://doi.org/10.1021/acs.langmuir.0c00573.
[22] C. Cheng, W. Song, Q. Zhao, H. Zhang, Halloysite nanotubes in polymer science: purification, characterization, modification and applications, Nanotechnol. Rev. 9 (2020) 323–344, https://doi.org/10.1515/NTREV-2020-0024/ASSET/GRAPHIC/J_NTREV-2020-0024_EQ_004.PNG.
[23] L.F. Atyaksheva, I.A. Kasyanov, Halloysite, natural aluminosilicate nanotubes: structural features and adsorption properties (A review), Petrol. Chem. 61 (2021) 932–950, https://doi.org/10.1134/S0965544121080119.
[24] M. Massaro, C.G. Colletti, G. Lazzara, S. Milioto, R. Noto, S. Riela, Halloysite nanotubes as support for metal-based catalysts, J. Mater. Chem. A 5 (2017) 13276–13293, https://doi.org/10.1039/c7ta02996a.
[25] S. Kadanyo, C.N. Matindi, N.N. Gumbi, D.S. Dlamini, Y. Hu, Z. Cui, B. He, B. B. Mamba, J. Li, Halloysite nanotubes for regulating thermodynamics and kinetics of polysulfone/poly (ethylene-co-vinyl alcohol) membranes with enhanced permeability, npj Clean Water 6 (2023) 19, https://doi.org/10.1038/s41545-023-00223-3.
[26] R.D. Sagare, F.S. Dasankoppa, H.N. Sholapur, K. Burga, Halloysite nanotubes: design, characterization and applications. A review, FARMACIA 69 (2021) 208–214, https://doi.org/10.31925/farmacia.2021.2.3.
[27] D. Rawtani, Y.K. Agrawal, Multifarious applications of halloysite nanotubes: a review, Rev. Adv. Mater. Sci. 30 (2012) 282–295.
[28] Y. Lvov, E. Abdullayev, Functional polymer-clay nanotube composites with sustained release of chemical agents, Prog. Polym. Sci. 38 (2013) 1690–1719, https://doi.org/10.1016/j.progpolymsci.2013.05.009.
[29] M. Hanif, F. Jabbar, S. Sharif, G. Abbas, A. Farooq, M. Aziz, Halloysite nanotubes as a new drug-delivery system: a review, Clay Miner. 51 (2016) 469–477, https://doi.org/10.1180/claymin.2016.051.3.03.
[30] S. Leporatti, Halloysite clay nanotubes as nano-bazookas for drug delivery, Polym. Int. 66 (2017) 1111–1118, https://doi.org/10.1002/pi.5347.
[31] M. Massaro, P. Poma, G. Cavallaro, F. García-Villén, G. Lazzara, M. Notarbartolo, N. Muratore, R. Sánchez-Espejo, C. Viseras Iborra, S. Riela, Prodrug based on halloysite delivery systems to improve the antitumor ability of methotrexate in leukemia cell lines, Colloids Surf. B Biointerfaces 213 (2022), https://doi.org/10.1016/j.colsurfb.2022.112385.
[32] G. Fakhrullina, E. Khakimova, F. Akhatova, G. Lazzara, F. Parisi, R. Fakhrullin, Selective antimicrobial effects of Curcumin@Halloysite nanoformulation: a Caenorhabditis elegans study, ACS Appl. Mater. Interfaces 11 (2019) 23050–23064, https://doi.org/10.1021/acsami.9b07499.
[33] X. Luo, J. Zhang, Y.-P. Wu, X. Yang, X.-P. Kuang, W.-X. Li, Y.-F. Li, R.-R. He, M. Liu, Multifunctional HNT@Fe 3 O 4 @PPy@DOX nanoplatform for effective chemo-photothermal combination therapy of breast cancer with MR imaging, ACS Biomater. Sci. Eng. 6 (2020) 3361–3374, https://doi.org/10.1021/acsbiomaterials.9b01709.
[34] M. Massaro, C.G. Colletti, G. Lazzara, S. Riela, The use of some clay minerals as natural resources for drug carrier applications, J. Funct. Biomater. 9 (2018) 58, https://doi.org/10.3390/jfb9040058.
[35] S.R. Levis, P.B. Deasy, Characterisation of halloysite for use as a microtubular drug delivery system, Int. J. Pharm. 243 (2002) 125–134, https://doi.org/10.1016/S0378-5173(02)00274-0.
[36] W. Li, D. Liu, H. Zhang, A. Correia, E. Mäkilä, J. Salonen, J. Hirvonen, H.A. Santos, Microfluidic assembly of a nano-in-micro dual drug delivery platform composed of halloysite nanotubes and a pH-responsive polymer for colon cancer therapy, Acta Biomater. 48 (2017) 238–246, https://doi.org/10.1016/j.actbio.2016.10.042.
[37] Z. Jiang, S. Sun, J. Liu, X. Sun, Recent advances of halloysite nanotubes in biomedical applications, Small (2023) 2306169, https://doi.org/10.1002/smll.202306169.
[38] S. Satish, M. Tharmavaram, D. Rawtani, Halloysite nanotubes as a nature's boon for biomedical applications, BJGP Open 6 (2019) 1–16, https://doi.org/10.1177/1849543519863625.
[39] Y. Lvov, W. Wang, L. Zhang, R. Fakhrullin, Halloysite clay nanotubes for loading and sustained release of functional compounds, 1227–1250, https://doi.org/10.1002/adma.201502341, 2016.
[40] J. Huang, Z.H. Tang, X.H. Zhang, B.C. Guo, Halloysite Polymer Nanocomposites, first ed., Elsevier Ltd., 2016 https://doi.org/10.1016/B978-0-08-100293-3.00021-2.
[41] Y. Jiang, P. Wang, J. Zheng, Use of ionic monomers to prepare halloysite polymer nanocomposites with reinforced mechanical performance, Appl. Clay Sci. 141 (2017) 248–256, https://doi.org/10.1016/j.clay.2017.03.003.
[42] M. Massaro, R. Noto, S. Riela, Halloysite Nanotubes: smart nanomaterials in catalysis, Catalysts 12 (2022) 149, https://doi.org/10.3390/catal12020149.
[43] M. Tharmavaram, G. Pandey, D. Rawtani, Surface modified halloysite nanotubes: a flexible interface for biological, environmental and catalytic applications, Adv. Colloid Interface Sci. 261 (2018) 82–101, https://doi.org/10.1016/j.cis.2018.09.001.
[44] A. Karewicz, A. Machowska, M. Kasprzyk, G. Ledwójcik, Application of halloysite nanotubes in cancer therapy—a review, Materials 14 (2021) 2943, https://doi.org/10.3390/ma14112943.
[45] S. Moghari, S.H. Jafari, M.K. Yazdi, M. Jouyandeh, A. Hejna, P. Zarrintaj, M. R. Saeb, In-out surface modification of halloysite nanotubes (Hnts) for excellent cure of epoxy: chemistry and kinetics modeling, Nanomaterials 11 (2021) 1–29, https://doi.org/10.3390/nano11113078.
[46] A.-R. Masoud, F. Alakija, M.J. Perves Bappy, P.A.S. Mills, D.K. Mills, Metallizing the surface of halloysite nanotubes—a review, Coatings 13 (2023) 542, https://doi.org/10.3390/coatings13030542.
[47] Y. Yang, Y. Chen, F. Leng, L. Huang, Z. Wang, W. Tian, Recent advances on surface modification of halloysite nanotubes for multifunctional applications, Appl. Sci. 7 (2017) 1215, https://doi.org/10.3390/app7121215.
[48] Z. Khoshraftar, F.S. Taheri, S. Nezami, A. Ghaemi, Using halloysite nanotubes modified by tetraethylenepentamine for advanced carbon capture: experimental and modeling via RSM and ANNs, Chem. Eng. J. Adv. 16 (2023) 100543, https://doi.org/10.1016/j.ceja.2023.100543.
[49] G. Kamińska, B. Dave, A.N.S. Appiah, J. Majewska, Exploitation of bentonite and halloysite fixed bed columns – removal of organic micropollutants and microbiological regeneration, Desalination Water Treat. 322 (2025) 101113, https://doi.org/10.1016/j.dwt.2025.101113.
[50] K. Shukla, V. Mishra, J. Singh, V. Varshney, R. Verma, S. Srivastava, Nanotechnology in sustainable agriculture: a double-edged sword, J. Sci. Food Agric. 104 (2024) 5675–5688, https://doi.org/10.1002/jsfa.13342.
[51] E. Dasi, M. Rudmin, S. Banerjee, Glauconite applications in agriculture: a review of recent advances, Appl. Clay Sci. 253 (2024) 107368, https://doi.org/10.1016/j.clay.2024.107368.
[52] H. Wei, H. Wang, H. Chu, J. Li, Preparation and characterization of slow-release and water-retention fertilizer based on starch and halloysite, Elsevier B.V, https://doi.org/10.1016/j.ijbiomac.2019.04.183, 2019.
[53] G. Teng, C. Chen, X. Ma, H. Mao, X. Yuan, H. Xu, Z. Wu, J. Zhang, Spherical assembly of halloysite clay nanotubes as a general reservoir of hydrophobic pesticides for pH-responsive management of pests and weeds, Small (2024), https://doi.org/10.1002/smll.202402921.
[54] J. Huang, L. Chen, M. Huang, M. Liu, Urea intercalated halloysite/sodium alginate composite hydrogels for slow-release fertilizers, Appl. Clay Sci. 242 (2023) 107041, https://doi.org/10.1016/J.CLAY.2023.107041.
[55] N. Asadi, R. Naderi, M. Mahdavian, Doping of zinc cations in chemically modified halloysite nanotubes to improve protection function of an epoxy ester coating, Corros. Sci. 151 (2019) 69–80, https://doi.org/10.1016/j.corsci.2019.02.022.
[56] Q.F. Gillani, F. Ahmad, P.S. Melor, M.I.A. Mutlib, S. Ullah, A synergy study of zinc borate in halloysite nanotube reinforced, siloxane epoxy base intumescent fire resistive coatings, Mater. Werkst. 49 (2018) 420–426, https://doi.org/10.1002/mawe.201700254.
[57] P. Maximov, E. Dasi, N. Kalinina, A. Ruban, B. Pokidko, M. Rudmin, Zinc-intercalated halloysite nanotubes as potential nanocomposite fertilizers with targeted delivery of micronutrients, Materials 16 (2023) 6729, https://doi.org/10.3390/ma16206729.
[58] I. Khitrin, P. Maximov, E. Dasi, K. Ibraeva, K. Ponomarev, N. Maximova, P. Belousov, A. Ruban, M. Rudmin, Glauconite-based nanocomposites with Zn/Cu/B: multifunctional micronutrient fertilizers, Minerals 15 (2024) 1–18, https://doi.org/10.3390/min15010012.
[59] C. Wang, Z. He, Y. Liu, C. Zhou, J. Jiao, P. Li, D. Sun, L. Lin, Z. Yang, Chitosan-modified halloysite nanotubes as a controlled-release nanocarrier for nitrogen delivery, Appl. Clay Sci. 198 (2020) 105802, https://doi.org/10.1016/J.CLAY.2020.105802.
[60] L. Fu, D. Fan, J. Zhang, P. Ouyang, J. Fan, H. Yang, Microstructure and properties of halloysite nanotubes and modification methods: a comprehensive review, Appl. Clay Sci. 253 (2024) 107348, https://doi.org/10.1016/j.clay.2024.107348.
[61] M. Salimi, E. Motamedi, B. Motesharezedeh, H.M. Hosseini, H.A. Alikhani, Starch-g-poly(acrylic acid-co-acrylamide) composites reinforced with natural char nanoparticles toward environmentally benign slow-release urea fertilizers, J. Environ. Chem. Eng. 8 (2020) 103765, https://doi.org/10.1016/j.jece.2020.103765.
[62] M. Huang, J. Huang, H. Yu, Q. Fangzhang, M. Liu, Assessment of the phytotoxicity of HNTs on two plants, Cynodon dactylon and Brassica rapa L, Environ. Sci. Nano 11 (2024) 3066–3079, https://doi.org/10.1039/d3en00897e.